The Conditions for Void Initiation in Metal Matrix Composites

I. Sabirov[1], D. Duschlbauer[2], H.E. Pettermann[2], O. Kolednik[1]

[1] Erich Schmid Institute of Materials Science, Austrian Academy of Sciences, Leoben, Austria
[2] Institute of Light Weight Structures and Aerospace Engineering, Vienna University of Technology, Vienna, Austria

ABSTRACT: *The conditions for void initiation in aluminum based metal matrix composites in under- and peak-aged conditions with a varying volume fraction of alumina particles are studied. A digital image analysis system is applied to perform a quantitative analysis of the fracture surfaces from stereo image pairs. The crack tip opening displacement in the moment of void initiation, COD_{vi}, is determined as a function of the distance and the angle of the alumina particles nearest to the crack tip. For each individual particle, the stress tensor at the moment of void initiation is calculated from the solution of the HRR-field. A mean-field theory is employed to calculate the maximum normal stresses, $\sigma^{max\,part.}_{vi}$, in the particle. An extremely high scatter of the COD_{vi}-values is found; the $\sigma^{max\,part.}_{vi}$-values show a much lower scatter. The reasons for that are discussed.*

INTRODUCTION

In a particle reinforced metal matrix composite, voids are initiated either by particle fracture or by matrix particle decohesion. For understanding the fracture properties of these materials, it is essential to study the local conditions for void initiation. The idea of the present paper is to determine for individual particles the stress field in the moment of void initiation as a function of the polar coordinates of the particle with respect to the crack tip (distance r, angle to the crack plane, θ). In a first step, the HRR-field-theory is employed, providing a mesoscopic composite stress tensor. In a second step, a Mori-Tanaka type mean field approach is employed to estimate the stress field acting in the particle.

MATERIAL, EXPERIMENTAL PROCEDURE AND RESULTS

Material properties

The material for this investigation is a cast and extruded MMC with an Al-6061 matrix and Al_2O_3 particles. The material was annealed 30 minutes at 560°C, quenched in water and aged at room temperature for the under-aged condition and at 160°C, 8 hours for the peak-aged condition. The chemical composition of the matrix is given in Table 1. The particle volume fraction is varied: f_{Al2O3} = *10, 15,* and *20%*. The mean particle diameter is about *10* µm.

Compact tension (CT) specimens with a thickness *B = 12.5* mm, a width of *W = 40* mm and an initial crack length of *a ≈ 20* mm were machined; the specimens had an LT crack plane orientation. Fracture mechanics tests are conducted on the pre-fatigued specimens according to the ESIS standard [1]. The results of the tests are collected in Table 2; the fracture initiation toughness is given in terms of the critical J-integral, $J_{0.2/Bl}$, and in terms of the critical stress intensity, K_{IC}. In the table, the tensile testing data are also listed: the Young's modulus, E, the yield stress, σ_y, the ultimate tensile strength, σ_u, and the strain hardening coefficient, N. σ_0 is a reference stress needed for the HRR-field estimates which is determined according to [1]. The values for the Al-6061 matrix material are given for comparison.

TABLE 1: Chemical composition of the Al-6061 alloy

Si	Fe	Cu	Mn	Mg	Zn	Cr	Ti
0.4÷0.8	0.7	0.15÷0.4	0.15	0.8÷1.2	0.25	0.04÷0.35	0.15

TABLE 2: Global material properties in under- and peak-aged conditions

% Al_2O_3	E [GPa]	σ_y [MPa]		σ_u [MPa]		N [MPa]		$J_{0.2/Bl}$ [kJ/m²]		K_{IC} [MPa√m]		σ_0 [MPa]	
		under	peak	under	peak	under	peak	under	peak	under	peak	under	peak
0	71	97	173	183	228	5.0	8.3	150	64	109	71	79	173
10	86	159	205	265	277	6.25	7.7	10.4	6.5	32	25	138	187
15	95	158	251	256	299	6.67	11.1	6.5	2.8	26	20	137	237
20	104	172	251	261	298	7.14	11.1	6.5	3.7	26	19	151	237

Local properties

An automatic fracture surface analysis system [2, 3] is used to analyze quantitatively the fracture surfaces and to get information on the distance and the position of the first particle from the crack tip. From the analysis of the corresponding regions on both specimen halves, crack profiles are extracted perpendicular to the pre-fatigue crack front so that each profile crosses a particle that is situated near the crack front. From the crack profiles, the critical crack tip opening displacement, COD_i, and the crack tip opening in the moment of void initiation, COD_{vi}, are determined. For each sample, between 10 and 20 particles are analyzed. A more detailed description of this procedure is given in [4].

As one can see from Fig.1, the scatter of the COD_{vi}-values is extremely high; for example, for the under-aged specimen with *10% Al$_2$O$_3$*, the values vary between *0* and *13* μm. Some of the particles fracture at a very low values of $COD_{vi} \approx 0$. A tendency to decreasing COD_{vi}-values with increasing angle, θ, is observed for all investigated specimens (but some particles located at low angles and fractured at $COD_{vi} \approx 0$ are observed, as well). As was described in [4], the reason might be related with the effect of the plastic zone which has a maximum extension at an angle of about $\theta = 70°$ with respect to the crack plane.

No clear dependency of COD_{vi} on the particle size or the distance to the crack tip is observed. The COD_{vi} vs. *r* curves show a scatter similar to those of Fig. 1. In most cases, the mechanism of void initiation is particle fracture. Void initiation by matrix-particle decohesion appears rarely and typically for relatively small particles.
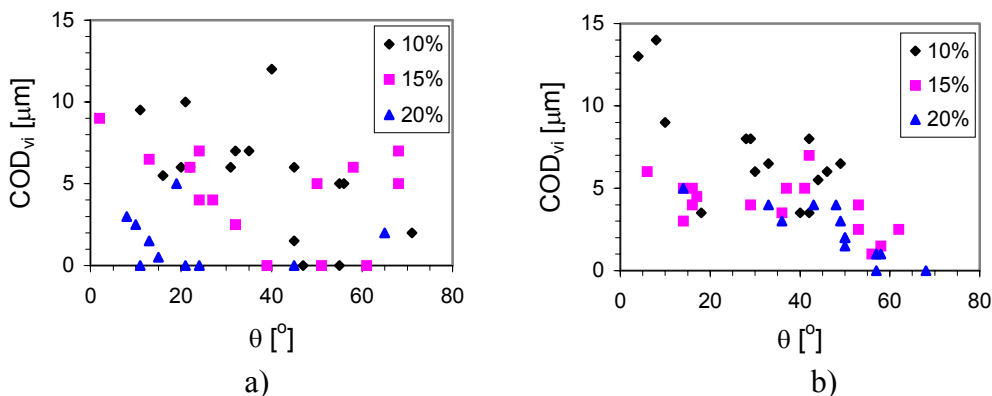

a) b)

Figure 1: Crack tip opening displacement at the moment of void initiation, COD_{vi}, vs. angle with respect to the crack plane, θ, for
a) under-aged conditions and b) peak-aged conditions.

The composite stress tensor at the point of void initiation

The composite stress tensor $\sigma_{ij,vi}$ at the moment of void initiation is calculated by means of the HRR- theory, providing the global stress field of the composite material as a function of the *J*-integral, the relative (particle) position to the crack tip (r, θ), and material parameters, such as the reference stress, σ_o, the coefficient α which is often set to 1, the Young modulus, *E*, and the strain hardening coefficient *N* [5, 6]

$$\sigma_{ij} = \sigma_0 \left[\frac{E\,J}{\alpha\sigma_0{}^2 I_N\, r} \right]^{1/(N+1)} \tilde{\sigma}_{ij}(N,\theta).$$ (1)

The values of dimensionless function σ_{ij} *(N, θ)* are taken from [7]. A power-law stress-strain behavior of the material is assumed

$$\varepsilon_{eq} = \frac{\sigma_0}{E} \left(\frac{\sigma_{eq}}{\sigma_0} \right)^N .$$ (2)

For each particle, the value of the *J*-integral in Eq. (1) is substituted by COD_{vi}, applying the relation

$$J = \frac{1}{d_N} \sigma_0\, COD,$$ (3)

where d_N is a dimensionless constant depending on the strain hardening coefficient, *N*, and on σ_0 /E [8].

Because of the small strain assumption, the HRR-theory yields unrealistic results for a region close to the tip. However, for $r \geq 2COD$ the results from the HRR-theory come close to those of elastic-plastic finite element computations [9]. The condition $r \geq 2COD_{vi}$ is fulfilled for most particles. It should be noted that HRR-theory is based on a homogeneous material, with the material data taken from Table 2. Thus, the stress tensor calculated with Eq.(1) represents a "mesoscopic", homogenized composite stress, $\sigma^{composite}$.

The particle stress tensor at the point of void initiation

For estimating the local phase stresses, $\sigma^{particle}$ and σ^{matrix}, a Mori-Tanaka type mean field approach [10, 11, 12] is employed where the micro-fields within each constituent are approximated by their phase averages. This method is based on micro-mechanical considerations and accounts for the

different properties of matrix and inclusion, the inclusion shape and orientation, and the inclusion volume fraction. The constituents stress fields are linked to the global composite stress field by fourth order stress concentration tensors, $\boldsymbol{B}$. The localization relations for the stress-fields take the form

$$\boldsymbol{\sigma}^{particle} = \mathbf{B}^{particle} \boldsymbol{\sigma}^{composite}$$
$$\boldsymbol{\sigma}^{matrix} = \mathbf{B}^{matrix} \boldsymbol{\sigma}^{composite}$$

$$(4)$$

As the stress concentration tensors, $\boldsymbol{B}$, are functions of the secant modulus of the matrix which in turn depends on the matrix stress tensor, $\boldsymbol{\sigma}^{matrix}$, an iterative solution procedure is employed. The particles are assumed to be spheres and remain linear elastic. The matrix behaves non-linear elastically according to a power-law (compare Eq.(2)). The matrix material is represented by a linear elastic comparison material, whose elastic modulus is chosen to coincide with the secant modulus (ratio of σ_{eq} over ε_{eq}) of the matrix material. The equivalent matrix stress, σ_{eq}, is not derived directly from the average matrix stress, $\boldsymbol{\sigma}^{matrix}$, which does not take into account local fluctuations of the matrix stress field, but by means of a second order theory [13,14].
One should be aware of the fact that inherent to the Mori-Tanaka theory is a uniform external stress field and that this criterion is violated in the vicinity of the crack tip as there are stress gradients located there. But for $r \geq 2COD_{vi}$ the stress gradient is not very large [9].


DISCUSSION

There might be different reasons for the high scatter of the COD_{vi}-values. Some of the particles could be pre-damaged or broken during the fabrication of the material, leading to near-zero COD_{vi}-values. As was mentioned above, alumina particles are considered as homogeneous spheres in our calculations. In reality, they are brittle, anisotropic single crystals with different possible cleavage planes [15]. In the investigated composites, the alumina particles are distributed without a preferred orientation. The type and the orientation of the cleavage planes have not been investigated so far.
As one can see from Fig. 2, the scatter of the $\sigma^{max\ part.}_{vi}$-values in all investigated samples is much lower in comparison with the scatter of COD_{vi}-values (Fig.1). The stresses vary between 700 and 900 MPa for the peak-aged material and between 600 and 800 MPa for the under-aged

material. The $\sigma^{max\ part.}_{vi}$-values are nearly independent of the angle to the crack plane, θ. A slight decrease of the $\sigma^{max\ part.}_{vi.}$-values with an increase of the distance r is observed, see Fig. 3.

It should be noted that the COD_{vi}-values can be measured with a relative accuracy of a few *%*. For a particle with a large angle θ, a step appears on both fracture surfaces. The COD_{vi}-value is measured as the height differences of the two steps. Assuming, for example, a step height of $\approx 20\mu$m, it is conceivable that a value of $COD_{vi} \approx 0.2$ μm might not be resolved. A $COD_{vi} = 0.2$ μm would result in a maximum void initiation stress of $\sigma^{max\ part.}_{vi} \approx 450$ MPa. Therefore, all the zero values in Figs. 2,3 are not realistic, and the stress values mentioned above are used to calculate the average stresses in Tab. 3.

a)   b)
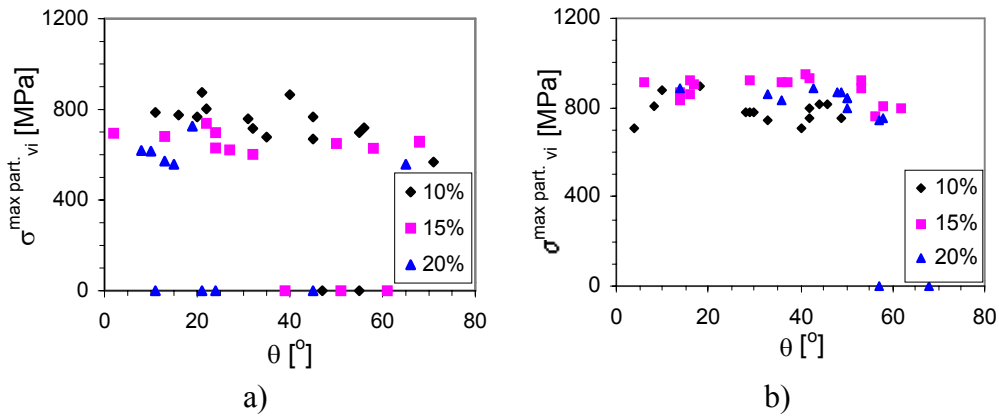
Figure 2: The $\sigma^{max\ part.}_{vi}$-values vs. angle with respect to the crack plane, θ, for a) under-aged and b) peak-aged samples.

a)   b)
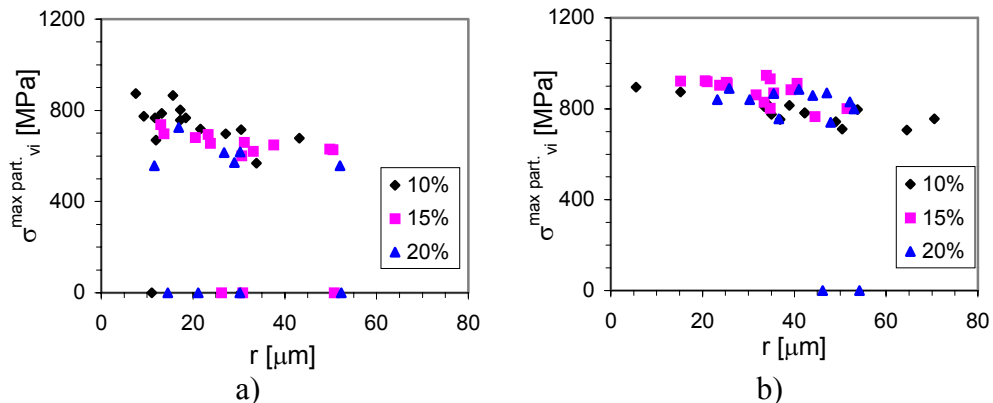
Figure 3: The $\sigma^{max\ part.}_{vi}$-values vs. distance between crack tip and particle, r, for a) under-aged and b) peak-aged samples.

TABLE 3: Conditions for void and fracture initiation at alumina particles near the crack front (average results) including near-zero data

% Al_2O_3	COD_{vi} [μm]		COD_i [μm]		$\sigma^{max\,part.}_{vi}$ [MPa]			
					HRR-theory		Mean-field	
	under	peak	under	peak	under	peak	under	peak
10	5.5± 3.4	7.2±3.2	10.7±6.3	12.2±3.4	589±121	700±52	709±126	787±52
	6.3± 2.8	7.2±3.2	12.2±5.1	12.2±3.4	624±82	700±52	746±80	787±52
15	4.4±2.9	4.0±1.6	6.4±4.6	8.9±3.9	517±100	761±58	615±96	882±55
	5.6±1.8	4.0±1.6	8.1±3.5	8.9±3.9	563±48	761±58	660±40	882±55
20	1.5±1.7	2.3±1.6	6.1±4.5	6.2±3.7	464±109	667±149	544±94	775±151
	2.4±1.5	2.8±1.4	6.1±4.5	7.3±2.8	540±64	725±53	607±64	834±50

Table 3 shows the average values of COD_{vi}, COD_i, and $\sigma^{max\,part.}_{vi}$. For each material, in the first row the mean values with the near-zero values are listed, below those without the near-zero values. Aging leads to increasing average particles stress values. Quite low average particles stresses in the under-aged sample with $f_{Al2O3} = 20\ \%$ are caused by the presence of a relatively large amount of particles which are broken at near-zero stresses. The difference in the $\sigma^{max\,part.}_{vi}$-values of different samples could be related to residual stresses in the material which might originate during the fabrication. Residual stress measurements are currently undertaken.

CONCLUSIONS

The conditions for void initiation in an Al6061-based metal matrix composite with a varying volume fraction of alumina particles were studied. The material was used in under- and peak-aged conditions. With a system for quantitative fracture surface analysis, the crack tip opening displacement at void initiation, COD_{vi}, was measured for particles close to the crack tip. The maximum normal stresses in the particles in the moment of void initiation, $\sigma^{max\,part.}_{vi}$, were estimated applying the HRR-field approach and a mean-field theory.
Void initiation occurs by particle fracture; only in a few cases, matrix-particle decohesion is observed. An extremely high scatter of the COD_{vi} values is found in all specimens. On the contrary, the $\sigma^{max\,part.}_{vi}$ values show a rather small scatter. The $\sigma^{max\,part.}_{vi}$-values vary between 700 and 900 MPa for the peak-aged material and between 600 and 800 MPa for the under-aged material. However, some particles fracture at comparably low stresses,

$\sigma^{max\ part.}_{vi} \leq 450$ MPa. These might be pre-damaged particles, however, this is not fully clear. The influence of residual stresses, particle pre-damage and particle cleavage plane orientation have not been investigated so far.

ACKNOWLEDGEMENTS

REFERENCES

1   ESIS P2-92 (1992) ESIS Procedure for Determining the Fracture Behaviour of Materials. European Structural Integrity Society, Delft, The Netherlands.

2   Scherer, S., Werth, P., Pinz, A., Tatschl, A., Kolednik, O. (1999) In: *Electron Microscopy and Analysis 1999,* pp. 107-110, Kiely, C.J. (Ed.). Institute of Physics Publishing, Bristol, U.K.

3   Scherer, S., Kolednik, O. (2001) *Microscopy and Analysis* 70 (March), 15.

4   Kolednik, O., Sabirov, I. (2001). In: K. Ravi-Chandar, et. al., Advances in Fracture Research, Proceedings of ICF10, Elsevier, Oxford, UK, paper 410.

5   Hutchinson, J.W. (1968) *J. Mech. Phys. Solids* 16, 13.

6   Rice, J.R., Rosengren, G.F. (1968) *J. Mech. Phys. Solids* 16, 1.

7   Shih, C.F. (1983) Tables of HRR Singular Field Quantities, MRL E-147. Materials Research Laboratory, Brown University, Providence, RI, USA.

8   Shih, C.F. (1981) *J. Mech. Phys. Solids* 29, 305.

9   McMeeking, R.M., Parks, D.M. (1979) *ASTM STP* 668, 175.

10   Mori, T., Tanaka., K. (1973) *Acta Metall.* 21, 571.

11   Benveniste, Y. (1987) *Mechanics of Materials* 6, 147.

12   Pettermann, H.E., Böhm, H.J., Rammerstorfer, F.G. (1997) *Composites* 28B, 253.

13   Hu, G. (1996*) Int. J. Plast.* 12, 439.

14   Qiu, Y.P., Weng, G.J. (1992) *Int. J. Appl. Mechanics* 59, 261.

15   Azhdari, A., Nemat-Nasser, S. (1998) *Mechanics of Materials* 28, 247.